Influence of differences in orientational planar density on the growth of Pb on the i–Ag–In–Yb quasicrystal

Sam Coates
Surface Science Research Centre and Department of Physics, University of Liverpool, Liverpool, L69 3BX, UK and Department of Materials Science and Technology, Tokyo University of Science, 6 Chome–3–1 Niijuku, Katsushika City, Tokyo 125-8585

Ronan McGrath and Hem Raj Sharma
Surface Science Research Centre and Department of Physics, University of Liverpool, Liverpool, L69 3BX, UK

Metal adsorption upon the 3–fold and 5–fold symmetric surfaces of the *i*–Ag–In–Yb quasicrystal has led to the observation of unique growth modes. Here, we present a study of the growth of Pb upon the 2–fold *i*–Ag–In–Yb surface, where the growth mechanism is found to be different from those observed on the other, higher symmetry surfaces of the same system. Initial Pb atoms occupy non–chemically–specific surface sites before forming a row structure. At higher coverages, the Pb atoms form a dense wetting layer before 1D Pb chains of limited size are self–assembled as a second layer. We therefore consider the Pb atoms to exhibit a type of Stranski–Krastanov growth mode. Substrate–adsorbate interaction is favoured in the wetting layer, before adsorbate–adsorbate interaction promotes chain growth. The difference in growth modes upon the three high symmetry surfaces is discussed with respect to their respective atomic densities.

I. INTRODUCTION

Adsorption on quasicrystal surfaces often leads to the observation of interesting phenomena, including pseudomorphic growth of adsorbates or the observation of unique growth modes [1–14]. In particular, the high symmetry surfaces of the icosahedral (*i*–)Ag–In–Yb quasicrystal have proven a fruitful playground [15–19]. The structural model for *i*–Ag–In–Yb is based on *i*–Cd–Yb [20, 21], and allows unambiguous determination of surface structure and adsorption sites.

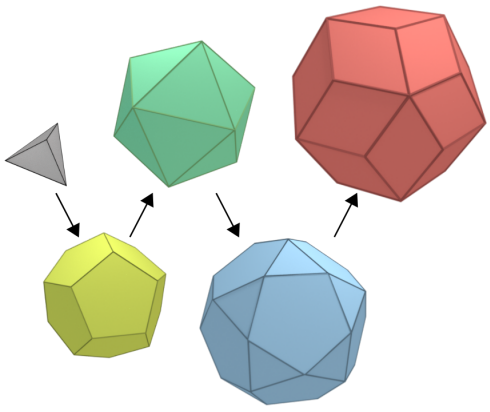

FIG. 1: Tsai cluster model. A hierarchical system of atomic shells form a large cluster. A rhombic triacontahedron (red) contains an icosidodecahedron (blue), an icosahedron (green), dodecahedron (yellow), and tetrahedron (grey). All shells are constructed from Ag/In atoms, except the 3$^{\text{rd}}$, which is Yb.

The *i*–Ag–In–Yb quasicrystal consists of a quasiperiodic arrangement of 'Tsai'–type clusters, a hierarchical system of atomic shells with icosahedral symmetry which are joined by rhombohedral 'glue' units [20]. In the *i*–Ag–In–Yb system, the shells are arranged as in Figure 1 where a Ag/In rhombic triacontahedron (red) contains a Ag/In icosidodecahedron (blue), an Yb icosahedron (green), Ag/In dodecahedron (yellow), and finally a Ag/In tetrahedron (grey). These shells are referred to as 5$^{\text{th}}$–1$^{\text{st}}$ respectively. The bulk quasicrystal can then be considered in terms of these 3D clusters, or, in terms of the 2D planes of atoms which are formed along the high symmetry directions of the icosahedral structure (2–fold, 3–fold, and 5–fold).

In previous work, this planar bulk structure model has been used to understand adsorption of metals on the high symmetry surfaces (3–fold, 5–fold) [15–17]. In these studies we considered a set of 'vacant' atomic planes above the surface truncation i.e. as if bulk growth to continue. Then, we compared the heights and motifs of adsorbed metal atoms to the heights and motifs of the atomic positions of these planes. In both the 3–fold and 5–fold systems, certain planes match with the experimental data, invoking the notion that these atoms are 'filling' particular vacant planes. In this manner, growth of Pb and Bi on the 5–fold surface was found to progress in a layer–by–layer fashion, whilst Pb on the 3–fold orientation formed 3D nanostructures [15–17]. The different growth modes observed on each surface were found to be related to the atomic density of the bulk model along

these particular orientations.

So far, the 2–fold surface of the *i*–Ag–In–Yb system has been comparatively under–utilised for adsorption studies – the same is generally true for other quasicrystals. An increased understanding of the atomic structure of this surface as obtained through bias–dependent Scanning Tunnelling Microscopy (STM) studies has now enabled such studies [22, 23]. Here, we report the adsorption of Pb on the 2–fold surface of *i*–Ag–In–Yb. Unlike on the other high symmetry surfaces, the Pb growth on the 2–fold surface cannot be understood by the planar adsorption model previously described. We see a Stranski–Krastanov type growth, with an initial dense wetting layer giving rise to a second layer consisting of 1D Pb chains. We compare these results to the other high symmetry systems, and explore its structure and stability of the observed growth mode in terms of atomic density and nearest neighbour distances.

II. METHODS

The 2–fold surface of an *i*–Ag–In–Yb QC was polished with successively finer grades of diamond paste (6–0.25 μm) before washing in methanol. The surface was then further cleaned with sputter–anneal cycles (30 minute Ar^+ sputter, 2 hour anneal at 700 K) under ultra–high vacuum, following previous studies which yielded clean surfaces with the expected bulk–truncated composition [22, 23]. Substrate cleanliness was monitored with low energy electron diffraction (LEED) and STM. Pb was evaporated at a constant flux of 120 nA onto the surface using a Focus EFM 3 evaporator.

III. RESULTS

A. Pb–dosed surface

1. *Low coverage Pb*

Figure 2(a) shows an STM image of the 2–fold Ag–In–Yb surface at negative bias, with approximately 0.15 monolayer (ML) of Pb deposited. Coverage was estimated by subtracting the area of the Pb protrusions from the total area of the scan. Under negative bias, the clean surface shows bright protrusions associated with Ag/In atoms [23]. Pb atoms are resolved as large protrusions in comparison to these bright surface atoms. Black circles indicate examples of surface atoms where the distinction between them and Pb atoms may be ambiguous. However, inset in Figure 2(a) is a height profile from the line indicated with an arrow, which shows the height difference between the brightest surface atoms and Pb atoms is ∼0.08 nm.

Dimers of Pb atoms are marked by white ovals and are numbered. Figure 2(b) is an enlarged section of a different STM scan taken at the same Pb coverage, with several other dimers numbered. The length and orientations of all the highlighted features in Figure 2(a, b) are shown in Table I. The orientations of dimers 1–6 are commensurate with the high symmetry directions of the 2–fold surface, which are marked on Figure 2(a) [22]. The angles of the dimers were measured with respect to the 2–fold symmetry axes of the surface, horizontal (0°) and vertical (90°), by drawing a line through the centre of the protrusions. The uncertainty in the process is reflected in the associated errors.The dimers constitute ∼70% of the Pb atoms observed at this coverage, calculated using STM images from 5 different areas. The remainder of the Pb atoms are either regarded as lone atoms or as dense areas with no defined geometry.

The Pb dimers of Figure 2(a, b) are recreated in the model shown in Figure 2(c), where black circles are Pb atoms and substrate atoms are represented by grey circles. The Pb dimers and their orientations suggest adsorption sites at the surface which are coloured corresponding to their shell. Here, we have assumed that each individual bright protrusion resolved in Figure 2(a) corresponds to a single Pb atom. This assumption is based on the average of measurements of the full–width at half maximum (FWHM) of individual protrusions, 0.6 ± 0.1 nm, and experience from several previous studies of Pb adsorption on quasicrystal surfaces [16, 17, 24].

The adsorption sites are shown enlarged in Figure 2(d). There are three types, characterized by their geometry: rectangular, pentagonal, and hexagonal (labelled as R, P, and H respectively). Hexagonal sites are exclusively formed by 5^{th} shell surface atoms (red), whilst 2^{nd} and 4^{th} shell atoms form rectangular sites (yellow, blue). The atomic constituents of the pentagonal sites varies, although they always include some 3^{rd} (green) and 5^{th} shell atoms. The sites for dimers 1 and 2 are only rectangular, while the other dimers can be formed by pairs of interchangeable sites, e.g. rectangular and hexagonal, or pentagonal and pentagonal, etc. Cluster centre and small triangular sites (labelled as CC and T in Figure 2(c)) are not considered as adsorption sites at this coverage: the observed separations of the Pb atoms do not consistently match those of cluster–centre sites, while the triangular sites are considered less favourable due to the smaller surface area of their midpoint. Likewise, if bridge or top sites were occupied, the distribution of Pb would be much denser with short Pb–Pb distances (~ 0.28 nm), and the exact type of site would be much more specific (i.e. Pb having to choose one particular bridge site over another).The separations and orientations of the model Pb atoms using these sites are shown in Table I, showing a good fit to those experimentally measured.

To further compare experimentally observed and model Pb adsorption, we have calculated autocorrelation

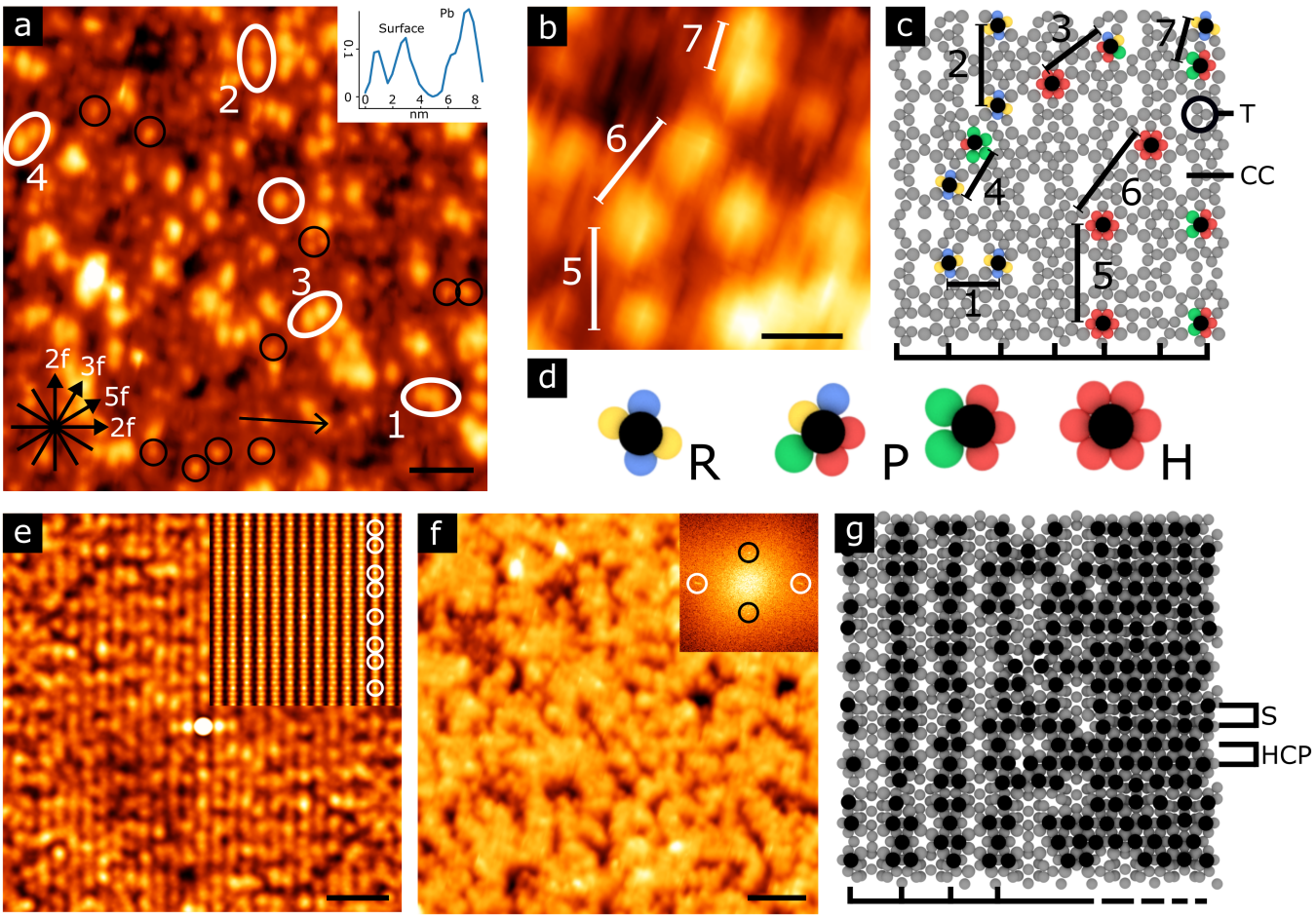

FIG. 2: (a) STM image (V_b = -2000 mV, I_t = 0.186 nA) of Pb atoms at a coverage of $\sim$ 0.15 ML. Pb atoms and dimers are highlighted in white, bright surface atoms are circled in black. Inset is a height profile taken from a line indicated by an arrow. Scale bar is 4 nm. (b) STM image (V_b = mV, I_t = nA) showing a close–up of Pb atoms. Marked are separations/dimer lengths. Scale bar is 2 nm. (c) Model schematic of the surface (grey), initial adsorption sites (coloured), and Pb atoms (black). Labelled are the various dimers from (a, b). T = triangular site, CC = cluster–centre site. (d) Enlarged models of the various adsorption sites. R = rectangular, P = pentagonal, H = hexagonal. The coloured circles correspond to the shells of the Tsai cluster in Figure 1. (e) Autocorrelation function taken from the extracted Pb positions from (a). Inset is an autocorrelation function taken from fully occupied adsorption positions from (c). Marked are spots of increased intensity which form a section of the Fibonacci sequence. Scale bar is 5 nm. (f) STM image (V_b = mV, I_t = nA) at a coverage of $\sim$ 0.75 ML. Inset is an FFT showing weak spots corresponding to vertical (white) and horizontal (black) rows. Scale bar is 8 nm. (g) Model schematic of the surface (grey) under increasing Pb deposition (black). Black bars at the bottom indicate the row–structure forming a dense overlayer. S = square–like 'band', HCP = HCP–like band.

functions for each. Figure 2(e) shows the autocorrelation function taken from the Pb atom positions extracted from Figure 2(a). A row structure with a horizontal separation of 1.2 $\pm$ 0.1 nm can be seen, with some disorder in the vertical direction of each row. To calculate the theoretical comparison, a set of model Pb atoms are arranged so that each rectangular, hexagonal, and pentagonal adsorption site of the surface is occupied along rows which do not contain a cluster centre (which we have previously discounted as initial adsorption sites). These 'adsorption rows' are indicated by black bars at the bottom of Figure 2(c). An example of the model Pb structure is shown on the left–hand side of Figure 2(g) with matching black bars. The autocorrelation function of the model Pb is then calculated, displayed as an inset in Figure 2(e). It also shows a 1.23 $\pm$ 0.07 nm row separation, matching the experimental data. The vertical structure in each row of the autocorrelation function is pronounced compared to the experimental function. This is likely due to the use of point–like objects when calculating the theoretical function compared to the comparatively poor resolution obtained along the vertical direction in the STM image.

	STM		Model	
Dimer	Δ (nm)	α (°)	Δ (nm)	α (°)
1	1.25 ± 0.06	1 ± 3	1.26	0.0
2	2.03 ± 0.09	89 ± 2	2.03	90.0
3	1.50 ± 0.03	33 ± 3	1.44	31.7
4	1.20 ± 0.06	60 ± 4	1.20	58.3
5	2.5 ± 0.1	89 ± 3	2.53	90.0
6	2.55 ± 0.05	59 ± 4	2.53	58.3
7	1.03 ± 0.08	82 ± 2	0.99	82.5

TABLE I: (Left) Lengths and orientations of dimers shown in Figures 2(a, b). Angles are with respect to the horizontal (0°). (Right) Corresponding values from the adsorption site model.

The periodic row separation observed in both autocorrelation functions can be explained by the nature of the adsorption rows in the model. The distribution of every row in the horizontal direction, independent of its morphology in the vertical, can be described as periodic with a margin of error. However, we can also separate the rows into groups based on their morphology along the vertical direction. In this instance we treat rows with similar atomic distributions, yet which are shifted relative to each other along the vertical direction, as distinct. Each of the subsequent groups of rows can then be described by a quasiperiodic distribution, as expected. However, as no particular group offers any specifically attractive adsorption sites to the Pb atoms, the end result is the seemingly periodic autocorrelation functions. In other words, the loss of quasiperiodicity evidenced in the horizontal direction of the autocorrelation functions is brought about by the treatment of the rows as non-unique objects. This also explains the uncertainty in the row separation value of the model Pb autocorrelation function.

In contrast, the modulation along the vertical rows of the model autocorrelation function is quasicrystalline. An example is highlighted by white circles in the inset of Figure 2(e), where spots which are slightly brighter form a section of the Fibonacci sequence. Other rows also show quasicrystalline bright protrusions, but are not highlighted for clarity. Unlike the horizontal separation of the rows there is no potential for a smearing of the signal along the vertical direction. Although the sites are non–chemical specific, each type of site is distributed in a quasicrystalline fashion along individual rows. Likewise, the separation of sites is on a smaller length scale compared to the separation of the rows, so quasiperiodic order is observed within the sample size used. The absence of similar spots in the experimental autocorrelation can be attributed to the low coverage, or, low resolution of the Pb atoms.

Figure 2(f) shows an STM image at increased coverage, approximately 0.75 ML. Here, the Pb is densely packed with very few individual atoms resolved. The previous row structure is barely visible, although there is evidence within the inset FFT (spots highlighted by white circles), which corresponds to a real–space separation of 1.2 ± 0.1 nm. The remaining adsorption sites beyond those previously discussed are modelled in Figure 2(g), which is a representation of increasing Pb coverage. On the left–hand side, the 1.2 nm–separated Pb rows are filled. Moving from left to right, other geometrical adsorption sites between the rows are filled, including cluster centres and pentagonal sites containing 'glue' Yb positions (atoms which join Tsai–type clusters). The result is a dense film with two types of horizontal 'bands' of Pb atoms: an hexagonal close packed (HCP)–like structure separated by square–like rows, highlighted and labelled as HCP and S respectively. The separation between the centres of the HCP–like rows is ∼2.0 nm. Very weak spots highlighted by black circles in the experimental FFT support this value, giving a horizontal row separation of 2.14 ± 0.07 nm. Again, these 'bands' may be quasicrystalline in their distribution, but the film appears too dense to reflect this.

2. High coverage Pb

After dosing for a calculated coverage of ∼1.35 ML, a second and third Pb layer start to form. Figure 3(a) shows an STM image taken of the surface after 20 minutes of Pb exposure. Labelled in white are examples of second layer chains, where the adjacent integer corresponds to the number of Pb atoms which form each structure, 1–6. Individual Pb atoms are considered as protrusions with a line scan exhibiting a FWHM of ∼ 0.6 nm. The lengths of chains 2–6 are shown in Table II. Third layer atoms are highlighted with a black circle. An autocorrelation function taken from the extracted second layer Pb positions is shown in Figure 3(b), which displays a row structure. The horizontal separations of the rows (i.e. horizontal 2–fold direction Figure (2(a)) is 1.18 ± 0.08 nm, and there is poor structure in the vertical direction – as with the first layer (Figure 2(e)). However, in the real–space image, individual chains are often separated by smaller distances, as indicated in Figure 3(c), which shows three two–atom chains separated by 0.87 ± 0.02 nm.

As the underlying Pb layer is too dense to resolve individual atoms, the adsorption sites of the second layer are considered solely in terms of the motifs it forms. First, we note that the chains are exclusively oriented along the same crystallographic direction as the initial row structure of the first layer. Second, the maximum length of

Chain	STM Length (nm)	Model Length (nm)
2	0.53 ± 0.04	0.56
3	1.14 ± 0.08	1.11
4	1.59 ± 0.04	1.60
5	2.13 ± 0.09	2.18
6	2.63 ± 0.02	2.64
Δ_{avg}	0.54 ± 0.07	0.52

TABLE II: (Left) Length of Pb chains in the second layer. The integer refers to the supposed number of Pb atoms in each chain. (Right) Corresponding length of each chain from the model. Δ_{avg} refers to the average of the difference between consecutive distances (2–3, 3–4 etc.).

unbroken chains is 6 atoms (larger chains are very infrequently observed, never more than 8 atoms long). This is not a coverage dependent phenomenon, as a third layer grows before larger chains are observed, indicating an ample 'supply' of Pb.

To interpret this observation, Figure 3(d) shows a model of the first layer (black) with second layer atoms (yellow) on top. Here, we use triangular and square hollows in the first layer as adsorption sites – examples are highlighted by small white circles. Chains of 2–6 atoms long are labelled, and their lengths are shown in Table II, showing a good fit to the experimental values. The lengths of two and three atom chains can vary slightly depending on which rows they adsorb to, so an average is shown for both. The motif of three two–atom chains in Figure 3(c) is also recreated, highlighted in white. The horizontal separations of these chains is 0.83 ± 0.02 nm, in good agreement with the experimental value (±5%). Closer separations of chains are modelled by a set of 9 atoms below this motif in Figure 3(d). These are seldom observed by STM, most likely as they provide a base for third layer growth, which then hide the second layer atoms. The limited size of the chains can be explained by positions in the first layer which are marked by white arrows either end of a 6–atom chain in Figure 3(d). These positions destroy the sequence of geometric adsorption sites (HCP/square), naturally preventing linear chains of atoms longer than 6 atoms. The infrequently observed larger chains are therefore presumed to arise from defects in the first layer.

Despite the apparent abundance of HCP/square–like sites in the horizontal direction (as indicated by the HCP/square–like bands in Figure 2(g)), the chains grow along the vertical direction of the first layer. The motivation for this is unknown – it may be dictated by the surface potential, or some corrugation in the first layer that is not detected by STM, and therefore not replicated in the model. Nevertheless, the separation of individual horizontal rows of the first layer (marked by black bars on the right of Figure 3(d)) is approximately 0.52 nm. This corresponds to the average difference between consecutive chain lengths in Table 3, shown as Δ_{avg}.

Some Pb atoms of the second layer are mobile, indicating that although there is a preference for growth along one 2–fold direction, individual second layer atoms only weakly interact with the first layer. Figure 3(e) shows three successive STM images taken from an enlarged area of Figure 3(a), where the scan–time for each large–scale image was 110 seconds. White circles indicate positions in which Pb atoms disappear/appear over time, while white arrows highlight a chain which grows from 3 atoms to 4, then finally reduces to 2. No such behaviour was observed on the 3–fold or 5–fold surface. A possible explanation for this diffusion is discussed in the next section.

An example of a third layer of Pb atoms is highlighted by a black circle in Figure 3(a). Detailed analysis of its structure is difficult, as increasing coverage causes crystalline islands of Pb to grow. This behaviour is consistent with Pb deposition on the other high–symmetry surfaces [16, 17].

Conventional growth modes are described in terms of the adsorbate structure, which is in turn explained by the interface energy between substrate and adsorbate. At large interface energies (high strain) the adsorbate typically forms crystalline islands with a structure commensurate with its natural crystal form (Volmer–Weber) [25]. At low strain energies, layer–by–layer growth occurs, with structure dependent on the substrate (Frank–van der Merwe) [26, 27]. In the interim, where surface–adsorbate and adsorbate–adsorbate energetics are comparable, an initial layer(s) is grown before nucleation of islands on top (Stranski–Krastanov) [28, 29]. These islands will have the natural crystalline structure of the adsorbate. We describe the growth of Pb observed here as a type of Stranski–Krastanov mode, due to the similarities in morphology, i.e., an initial wetting layer is followed by growth preferred along z up to a third layer. However, as demonstrated, the second layer of Pb does not form its crystalline allotrope (i.e. FCC), hence, a modified Stranski–Krastanov growth is inferred.

B. Comparison to 3–fold and 5–fold systems

1. *Planar adsorption model*

Previous examples of Pb growth on the i–Ag–In–Yb system have been explained using a planar adsorption model. Here, certain planes of 'vacant' bulk atoms above the surface termination (i.e. if bulk growth were to continue) explain both the heights and topography of adsorbed Pb atoms [16, 17]. Figure 4(a–c) shows the pla-

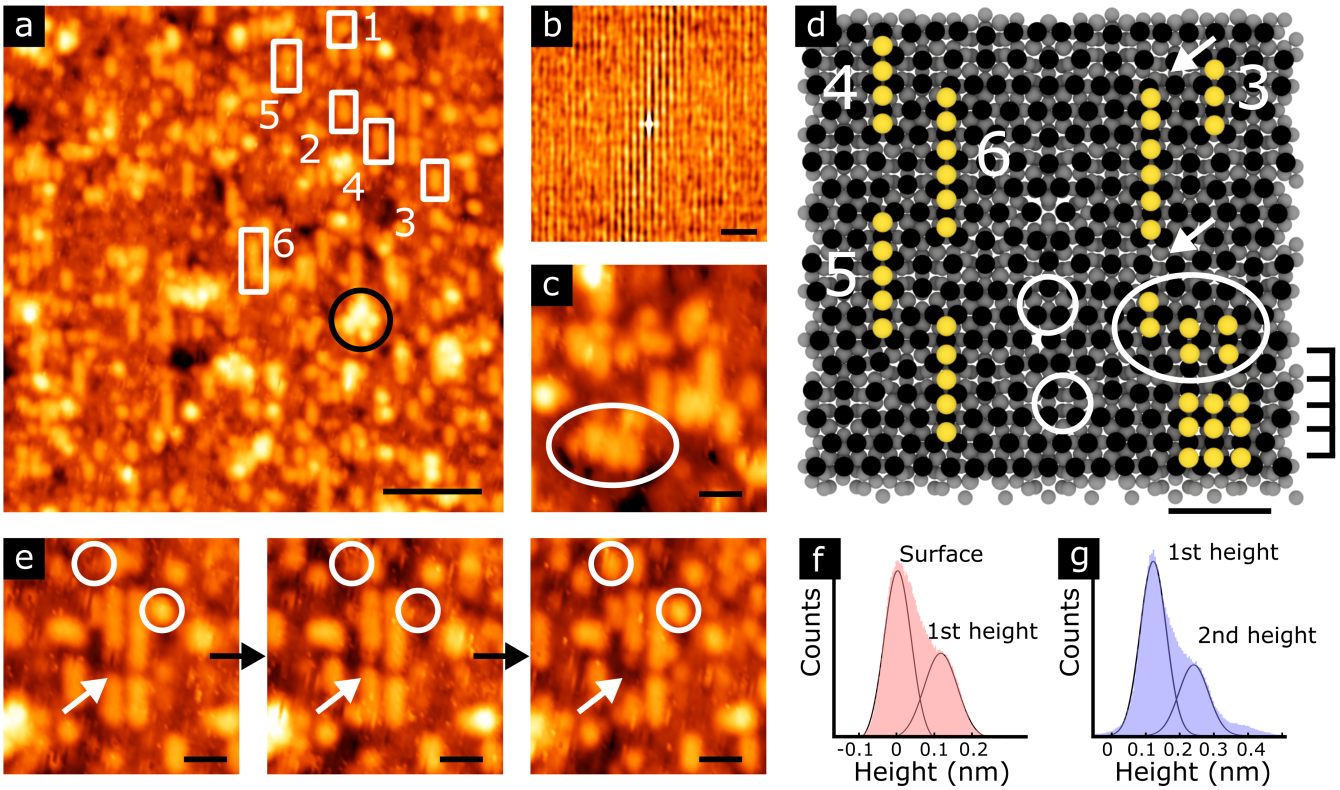

FIG. 3: (a) STM image (V_b = 200 mV, I_t = 0.411 nA) at a coverage of ∼1.3 ML. Second layer Pb chains are marked in white, with integers reflecting their length in terms of atoms. Third layer atoms are circled in black. Scale bar is 10 nm. (b) Auto correlation function taken from the extracted second layer Pb. Scale bar is 5 nm. (c) Enlarged section of (a) showing closely separated two–atom chains. Scale bar is 2 nm. (d) Model schematic of the second Pb layer (yellow) on top of the first (black). Triangular and square adsorption sites are marked by white circles. Lengths of chains are indicated by adjacent integers. White arrows indicate positions in the first layer which limit the length of unbroken chains. The motif in (c) is replicated, and indicated in white. A dense second layer formation is shown below. The horizontal row separation of the first layer is indicated by black bars on the right. Scale bar is 2 nm. (e) A series of STM images taken from the same area as (a), enlarged, showing diffusion of individual second layer Pb atoms. White circles show individual atoms appearing/disappearing, white arrows show a chain increasing/decreasing in length. Scale bar is 2 nm. (f) Height histogram from Figure 2(a). (g) Height histogram from Figure 3(a).

nar model for the 2–fold, 5–fold, and 3–fold orientations, with surface planes and heights of Pb atoms above the surface labelled. The planes are coloured to represent the shells as in Figure 1, where black bars represent the total density at those heights with planes consisting of multiple shells. Atomic density per surface plane decreases from left to right (2–fold to 3–fold) respectively. The 5–fold system (Figure 4(b)) shows only two adsorption planes/Pb heights to allow for direct comparison; further heights of Pb atoms on this surface are observed at larger z values.

Figure 3(f) is a histogram taken from Figure 2(a) showing the height difference between the substrate and the first height of Pb atoms, measured as 0.12 ± 0.02 nm. This value is calculated by fitting Gaussian peaks to the histogram (shown as the solid lines), setting the mean of the surface peak to a height of 0 nm, and consequently finding the mean of the Pb peak. If we assume that the electronic height measured is equivalent to the atomic height (as in previous work on the i–Ag–In–Yb system [16, 17]), we see that the height of the Pb atoms does not match any bulk plane above the surface termination, as shown in Figure 4(a). Similarly, Figure 3(g) shows a histogram taken from Figure 3(a), showing the difference in heights between the first and second layer of Pb, 0.13 ± 0.03 nm. This value is calculated using the peak–fitting method described above, where we set the mean of the first height Pb atom peak to 0.12 nm. The second height is also marked on Figure 4(a). It is close to a plane of 2^{nd} shell atoms, but, the morphology of this plane does not match with the second layer Pb chains constructed. Therefore, the growth of Pb on the 2–fold surface cannot be explained by the planar adsorption model.

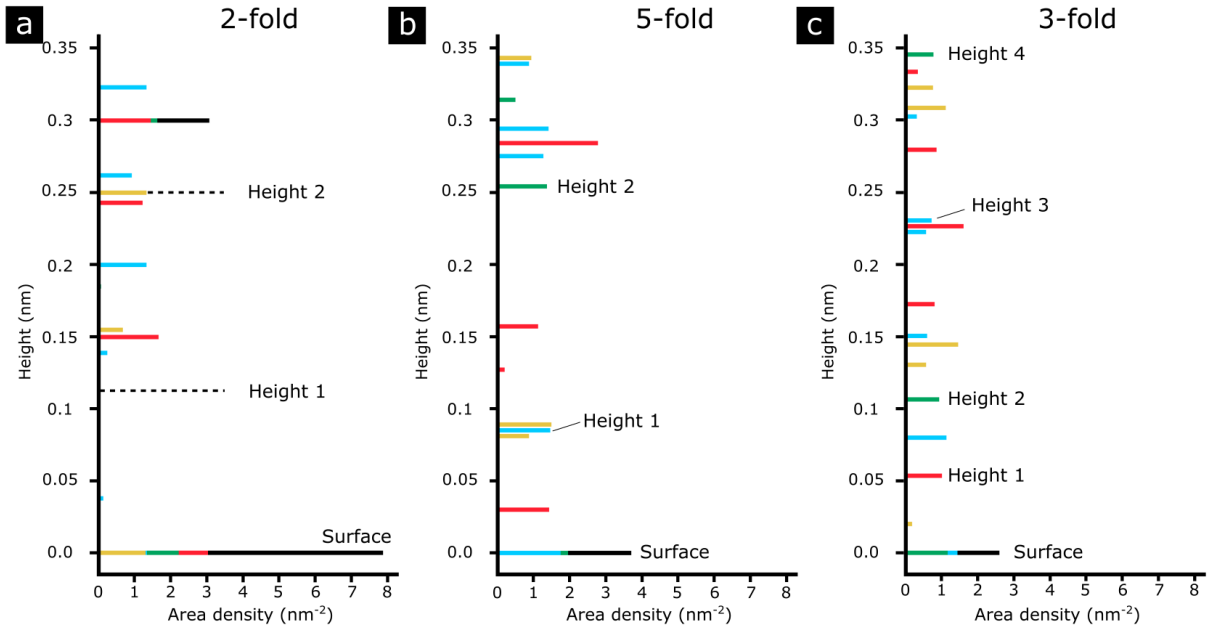

FIG. 4: Planar model of the i–Ag–In–Yb quasicrystal. y–axis is height above the surface truncation, x–axis is atomic density. The colours of the solid lines represent the shells of the Tsai–type cluster. The 2$^{\text{nd}}$ shell is yellow, 3$^{\text{rd}}$ green, 4$^{\text{th}}$ blue, and 5$^{\text{th}}$ red. The 1$^{\text{st}}$ shell atoms are omitted as their positions are not well defined at the surface. (a) The 2–fold direction with the surface plane labelled. Dashed lines represent the heights of the Pb layers observed. (b) A section of the 5–fold planar adsorption model. The surface and shells which correspond to Pb heights are labelled. (c) Corresponding diagram along the 3–fold direction.

2. *Directional atomic density*

The Pb systems on the 3–fold and 5–fold surface differ in their growth and 3D morphology. The 5–fold surface produces a multi–layer Pb film [17], whilst the 3–fold creates a sparse network of isolated nano–structures [16]. The difference between these modes has been attributed to the change in atomic density between the two high symmetry directions: in the bulk model, the 5–fold direction has, on average, more atoms per plane (more adsorption sites per plane), whilst the 3–fold has a higher density of planes perpendicular to the surface (more adsorption sites along the z direction).

Figure 4 shows that the 2–fold surface plane is the most dense of the system. It is also the only surface plane which contains atoms from every shell of the Tsai–type cluster; the other surface orientations consist of 3$^{\text{rd}}$ and 4$^{\text{th}}$ shell atoms only. This ultimately affects the chemistry of the surface planes. The ratio of the composition (Ag : In : Yb) of the 2–fold, 5–fold, and 3–fold surfaces are, respectively: (1 : 1.34 : 0.84), (1 : 3.97 : 1.90), (1 : 2.71 : 3.86), calculated using the method described in [22]. In other words, the chemical species distribution is more homogeneous upon the 2–fold surface. This may explain why the first layer Pb atoms adsorb at the hollows of geometric sites (hexagonal, pentagonal, rectangular) as opposed to sites with particular chemical environments, as with the 3–fold and 5–fold surfaces. This increase in surface density and lack of specificity may be the key factor in the different adsorption mode exhibited here.

3. *Nearest neighbours*

To understand the planar adsorption model, the stability of the Pb atoms on both the 3–fold and 5–fold surfaces were explained in terms of nearest neighbour distances in comparison to crystalline Pb. For instance, planes parallel to the 3–fold direction have atomic positions with nearest neighbour distances larger than that of crystalline Pb (0.32 nm), suggesting that in–plane (layer–by–layer) growth would be unstable. However, certain planes perpendicular to the 3–fold direction give positions with similar or smaller distances to 0.32 nm, thus promoting out–of–plane growth [16]. This is a reflection on the directionally dependent atomic density of the system. We therefore employ a similar method by considering the atomic density of the 2–fold surface and subsequent nearest neighbour distances to explain the Pb structure and explore its stability.

We can use the models shown in Figures 2(g) and 3(d)

to calculate the surface–Pb and Pb–Pb nearest neighbour distances to consider the stability of the film. To do so, Pb atoms are placed at their proposed adsorption sites at the measured heights above the model substrate. Then, the average nearest neighbour distances between the surface and first layer, first and second layer, and intra–layers are measured.

The distance between the surface and the first layer is 0.34 ± 0.03 nm, approximately the nearest neighbour distance of crystalline Pb, indicating a strong interaction. This separation is smaller at the rectangular and hexagonal sites of the adsorption rows (0.31–3.2 nm), which could explain the initial row structure observed. The intra–layer separation of Pb atoms in the first layer is 0.54 ± 0.04 nm, suggesting a weakly self–interacting layer. Both of these observations indicate that the first layer is stabilised by Pb atoms preferentially bonding to surface atoms. The nearest neighbour distance between the first and second layers is 0.36 ± 0.03 nm, again, a distance which is close to crystalline Pb. The second layer has the same intra separation as the first, ∼0.55 nm. This presumably indicates that the chains are weakly interacting, again aiding in the diffusion in some of the atoms.

IV. CONCLUSION

In this work, we have shown how Pb grows on the 2–fold surface of the *i*–Ag–In–Yb quasicrystal and compared these observations to the other high symmetry orientations. The 3–fold and 5–fold systems have previously been explained by a planar model which uses 'vacant' bulk planes to explain adsorption sites. On the 2–fold surface, Pb atoms do not follow this scheme, growing in a type of Stranski–Krastanov fashion by forming an initial dense wetting layer before growing linear chains in the second layer. The first layer can be explained by chemically non–specific geometric adsorption sites which give surface–Pb nearest neighbour values close to crystalline Pb. The second layer forms 1D chains with maximum lengths of 6 atoms, explained by the underlying structure of the first layer.

The different adsorption schemes of Pb across the high symmetry orientations of *i*–Ag–In–Yb has also been explored and compared. In all 3 systems unique growth is observed, the specific behaviour of which appears to change with the changing atomic density of the bulk orientation. It would be interesting to assess whether each type of growth phenomena is general across all Tsai–type quasicrystals and approximants, or is specific to the Ag–In–Yb phase.

ACKNOWLEDGEMENTS

Partial support for this work from the Engineering and Physical Sciences Research Council (grant number EP/D071828/1) and the European Integrated Centre for the Development of New Metallic Alloys and Compounds is gratefully acknowledged.

[1] V. K. Singh, M. Mihalkovic, M. Krajčí, S. Sarkar, P. Sadhukhan, M. Maniraj, A. Rai, K. Pussi, D. L. Schlagel, T. A. Lograsso, et al., Phys. Rev. Research **2**, 013023 (2020).

[2] S. Coates, J. A. Smerdon, R. McGrath, and H. R. Sharma, Nat. Commun. **9** (2018).

[3] J. Ledieu, É. Gaudry, V. Fournée, J. Smerdon, and R. D. Diehl, Zeitschrift für Kristallographie-Crystalline Materials (2017).

[4] R. McGrath, H. R. Sharma, J. A. Smerdon, and J. Ledieu, Phil. Trans. of R. Soc. A **370**, 2930 (2012).

[5] J. A. Smerdon, K. M. Young, M. Lowe, S. S. Hars, T. P. Yadav, D. Hesp, V. R. Dhanak, A. P. Tsai, H. R. Sharma, and R. McGrath, Nano Lett. **14**, 1184 (2014).

[6] V. Fournée, É. Gaudry, J. Ledieu, M.-C. De Weerd, D. Wu, and T. Lograsso, ACS Nano **8**, 3646 (2014).

[7] V. Fournée, J. Ledieu, M. Shimoda, M. Krajčí, H. R. Sharma, and R. McGrath, Israel Journal of Chemistry **51**, 1314 (2011).

[8] T. Cai, J. Ledieu, R. McGrath, V. Fournée, T. Lograsso, A. Ross, and P. Thiel, Surf. Sci. **526**, 115 (2003).

[9] K. J. Franke, H. R. Sharma, W. Theis, P. Gille, P. Ebert, and K. H. Rieder, Phys. Rev. Lett. **89**, 156104 (2002).

[10] J. Ledieu, J. T. Hoeft, D. E. Reid, J. A. Smerdon, R. D. Diehl, T. A. Lograsso, A. R. Ross, and R. McGrath, Phys. Rev. Lett. **92**, 135507 (2004).

[11] J. Ledieu, L. Leung, L. H. Wearing, R. McGrath, T. A. Lograsso, D. Wu, and V. Fournée, Phys. Rev. B **77**, 073409 (2008).

[12] R. Lüscher, M. Erbudak, and Y. Weisskopf, Surf. Sci. **569**, 163 (2004).

[13] K. Pussi, M. Gierer, and R. D. Diehl, Journal of Physics: Condensed Matter **21**, 474213 (2009).

[14] J. A. Smerdon, J. K. Parle, L. H. Wearing, T. A. Lograsso, A. R. Ross, and R. McGrath, Phys. Rev. B **78**, 075407 (2008).

[15] S. S. Hars, H. R. Sharma, J. A. Smerdon, S. Coates, K. Nozawa, A. P. Tsai, and R. McGrath, Surf. Sci. **678**, 222 (2018), ISSN 0039-6028.

[16] S. Coates, S. Thorn, R. McGrath, H. R. Sharma, and A. P. Tsai, Phys. Rev. Materials **4**, 026003 (2020).

[17] H. R. Sharma, K. Nozawa, J. A. Smerdon, P. J. Nugent, I. McLeod, V. R. Dhanak, M. Shimoda, Y. Ishii, A. P. Tsai, and R. McGrath, Nat. Commun. **4**, 2715 (2013).

[18] H. R. Sharma, J. A. Smerdon, P. J. Nugent, A. Ribeiro, I. McLeod, V. R. Dhanak, M. Shimoda, A. P. Tsai, and

R. McGrath, J. Chem. Phys. **140**, 174710 (2014).
[19] N. Kalashnyk, J. Ledieu, É. Gaudry, C. Cui, A. P. Tsai, and V. Fournée, Nano Research **11**, 2129 (2018).
[20] H. Takakura, C. P. Gómez, A. Yamamoto, M. de Boissieu, and A. P. Tsai, Nat. Mater. **6**, 58 (2007).
[21] A. P. Tsai, J. Q. Guo, E. Abe, H. Takakura, and T. J. Sato, Nature **408**, 537 (2000).
[22] C. Cui, P. J. Nugent, M. Shimoda, J. Ledieu, V. Fournée, A. P. Tsai, R. McGrath, and H. R. Sharma, Journal of Physics: Condensed Matter **26**, 015001 (2013).
[23] D. Burnie, S. Coates, R. McGrath, and S. H. R., Journal of Physics: Conference Series **1458**, 012017 (2020).
[24] J. Ledieu, M. Krajčí, J. Hafner, L. Leung, L. H. Wearing, R. McGrath, T. A. Lograsso, D. Wu, and V. Fournée, Phys. Rev. B **79**, 165430 (2009).
[25] M. Volmer and A. Weber, Zeitschrift für physikalische Chemie **119**, 277 (1926).
[26] F. C. Frank and J. H. van der Merwe, Proc. R. of Soc. Lond. A **198**, 205 (1949).
[27] F. Frank and J. H. Van der Merwe, Proc. R. of Soc. Lond. A **198**, 216 (1949).
[28] I. N. Stranski, Zeitschrift für Physikalische Chemie **136**, 259 (1928).
[29] I. N. Stranski and L. Krastanow, Monatshefte für Chemie und verwandte Teile anderer Wissenschaften **71**, 351 (1937).